ISME

Stability Investigation of Hydraulic Interconnected Suspension System of a Vehicle with a Quaternion Neural Network Controller

N. Palangsavar[*]
M.Sc. Student

A. R. Mamouri[†]
Instructor

Using hydraulic interconnected suspension (HIS) system to improve the stability of the vehicles is a matter of recent interest of many scholars. In this paper, application of this kind of suspension system and its impact on the stability of the vehicle are studied. The governing dynamic relations of the system are presented, using free body diagram, Newton-Euler motion equations, and relations related to the mass flow rate of fluid. By completing the design of the passive suspension system and the hydraulic interconnected suspension system and employing the half car model in the transverse direction with four degree of freedom, MATLAB® (V.8.1) /Simulink (MATLAB® is a software package produced by The Math Works, Inc.) software is used to investigate and compare the body and wheel responses of the vehicle in exposure to road surface roughness. In the end, quaternion neural network controller has been used due to the obtained nonlinear equations in interaction of suspension system as well as the coupled differential equations. Using quaternion neural network controller, the results indicated that the stability of vehicle and ride comfort are increased and also more smooth responses are generated.

Keywords: Quaternion Neural Network (QNN) Controller, Hydraulic Interconnected Suspension (HIS) System, Passive Suspension System, Vehicle Stability

1 Introduction

Over the years, the automotive industry has been pursued to enhance quality and increase the handling ability in vehicles [1]. Suspension system of vehicles, as a member in vehicles, has a main function in provision of ride comfort and rollover stability control [2]. This system must be able to absorb the vibration caused by road surface roughness (which is the main source of vibrations in the vehicle) and also keeps the balance of the vehicle through circuitous routes [3]. Suspension systems can be listed in terms of controllability, positioning, and wheels dependency or independency [4].

[*] Corresponding Author, M.Sc. Student, Higher Education Institute of Ishraq, Bojnourd, Iran
nabi.palangsavar@gmail.com
[†] Instructor, Department of Mechanical Engineering, Islamic Azad University, Bojnourd Branch, Bojnoud, Iran,
amirelmir3000@yahoo.com
Manuscript received January 22, 2019; revised February 14, 2019; accepted February 16, 2019.

Using a hydraulic interconnected suspension (HIS) system not only could augment rolling hardness along with rollover damping factor in vehicles, but also it could provide an ease of ride [5]. Miller and Nobles [6] used an elasticated rubber in their innovative suspension system called " Hydraulic Interconnected Suspension System" and then optimized it in the next design. The system did not include any fluid flow between the front and rear suspension systems under influence of vertical movement and roll angle, and instead, the gas in the upper compartment is compressed regarding the wheel movement. But, the fluid flow between the front and rear suspension systems reduces bounce motion (in fact, the pitch angle reduces) due to the impact of pitch angle. As a result, driving under the pitch angle will be improved in the suspension system developed by Miller and Nobles.

Allison [7] used a type of a mechanical interconnected suspension system with a trailing arm at the rear of the vehicle. In this suspension system, the amplitude of pitch angle is reduced due to a internal connection between the front wheels and the rear wheels. The main drawback of this suspension system was its low anti-rolling frequency as well as the loose control over the yaw angle during the dynamic load implementation. Esfahani et al. [8] and Zhang et al. [9] have modeled other types of passive and semi-active suspension systems with hydraulic interconnected concept and dynamic analysis. The mathematical model developed by these scholars to analyze and calculate the response of vehicle under vertical displacement and roll angle demonstrated that the resistance of a vehicle with such a suspension system to roll angle is higher than the conventional vehicles. In this system, a variable and self-leveling damper can be used to improve performance of the vehicle.

Cao et al. [10] also suggested an interconnected suspension system with a hydro-pneumatic feedback unit. The experimental and analytical methods used in this design revealed that using this suspension system in the vehicle will increase controllability of the rolling stability and travel comfort. The major problem with design of the hydro-pneumatic suspension system is the large diameter of the cylinder as well as initial dimensions and pressure of the reservoir, which makes it difficult to handle from design and maintenance standpoints. Zhu et al. [11] modeled and optimized the pitch angle of a pneumatically interconnected suspension (PIS) system. They presented a new method for analysis of mode and transmissibility properties. The optimization results revealed that this suspension system can reduce the pitch vibration. Pneumatic resonance frequency can be controlled by pipe length, pipe diameter and local loss factor in terms of the pipe parameters.

Zou et al. [12] simulated another type of a HIS system that was based on a hydraulic energy-regenerative shock absorber (HESA). The simulation results presented excellent softness of the vehicle and passenger comfort compared to the passive suspension system. Chen et al. [13] investigated the influence of key parameters of the HIS system on the vehicle’s dynamics and also carried out a validation based on available experimental data.

The results indicated that the slope of the roll angle and left-tire force in the z-axis direction is negatively correlated with the oil pressure. Furthermore, the key parameters of the HIS system have subtle impact on the maximum lateral acceleration. Bouazara and Richard [14], Bagheri et al.[15], Nariman-Zadeh et al. [16], and Thompson [17] have conducted numerous investigations on active suspension systems. The results of these scholars demonstrated that this type of suspension system creates an excellent design to redress the balance between the travel comfort and the hardness of the roll and pitch angles. These systems consist of hydraulic controllers and servo-mechanical valves [18]. Of course, high energy consumption in the active suspension system limits their general use in vehicles [19].

In this paper, the stability of a vehicle with an HIS system and a quaternion neural network controller is carried out. The governing relations of the system at dynamic state are expressed, using free body diagram, Newton-Euler motion, and fluid relations. Regarding selection of the MacPherson suspension system for the first vehicle, the values of the spring stiffness and the shock absorber damping are considered in the model analysis section.

While completing design of the hydraulic interconnected suspension system, the vehicle's body and wheels response to the road coarseness is investigated and compared with each other using MATLAB® (V.8.1)/Simulink (MATLAB® is a software package produced by The Math Works, Inc.) and considering the half car model with four degree of freedom in the transverse direction.

In the end, the quaternion neural network controller has been used in order to improve behavior of the HIS system due to the nonlinear equations obtained from the suspension system interaction and coupled differential equations. The main novelties of present study are as follows:

- Modeling and simulating half of the vehicle in transverse direction with the conventional passive suspension system in MATLAB® (V.8.1)/Simulink,
- Modeling and simulating half of the vehicle in transverse direction with the hydraulic interconnected suspension system in MATLAB® (V.8.1)/Simulink and
- Improving the stability performance of the vehicle by selecting quaternion neural network controller
- The overall schematic of the problem in previous studies is that the bottom chamber of the hydraulic cylinder of the left suspension is directly connected to the upper chamber of the hydraulic cylinder of the right suspension [13]. Since the lower and upper chambers of the cylinders do not have the same volume due to the presence of the piston rod; the controllability of the rolling stability of the vehicle would be difficult during movement if the cylinders are directly connected. This problem has been fixed in the designed model through this study (Illustrated in figure (1)). Also, the travel comfort and controllability of the rolling stability of the vehicle with current model have been improved dramatically in comparison with the passive suspension system.

2 Mathematical modeling and design of the proposed HIS system

2.1 System layout

In the well-known suspension systems like Citroen Xantia, typically four hydraulic cylinders with four hydro-pneumatic spheres are used. In the proposed suspension system, instead of four hydro-pneumatic spheres, four cylinders similar to the main cylinders are used. It is noteworthy to mention that the hydraulic cylinders used in this system are not fed by any external source (accumulator) and are completely in a closed hydraulic circuit, so that oil only flows within a circuit which is defined between the four hydraulic cylinders.

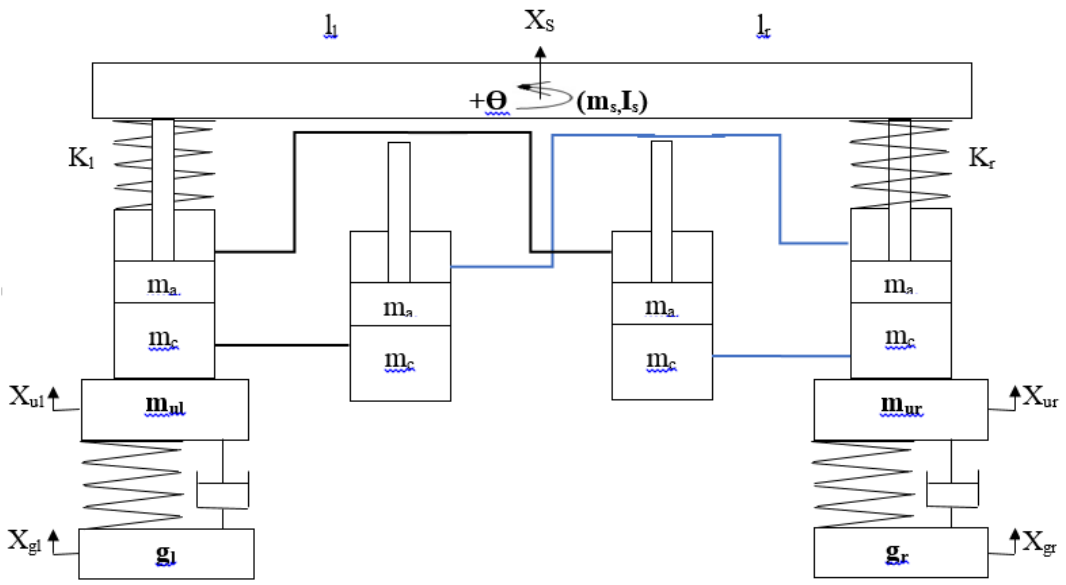

Figure 1 The proposed half car model in transverse direction with HIS system.

Figure (1) illustrates schematic of the proposed hydraulic suspension system. As shown in figure (1), the lower compartment of the left-hand hydraulic suspension cylinder should be connected to the upper compartment of the right-hand hydraulic suspension cylinder. This connection cannot be accomplished directly since the bottom and top of the cylinders do not have the same volume. It is noteworthy to mention that the main reason of unequal volume at both sides of the cylinder is the rod of the piston in the upper part of the cylinder.

Two other hydraulic cylinders with a same size are used in order to solve this issue. These two hydraulic cylinders only have a balancing role in volume and do not play a leading role in absorbing and damping the forces due to the weight and dynamics of the vehicle. For this purpose, the iso-volumetric parts (bottom part of the cylinder with the bottom part and upper part of the cylinder with the upper part) must be connected together.

2.2 Mathematical modeling of the HIS system

In order to evaluate the performance of the proposed hydraulic suspension system, first its mathematical model is extracted and then simulated in the MATLAB® (V.8.1)/Simulink software. In this scheme, two degrees of freedom are considered for sprung mass and only one degree of freedom is taken into consideration for each wheel of the vehicle. The Newton-Euler equations are used to express the behavior of the proposed model. The following equations can be expressed from the free body diagram depicted in figure (1):

Vertical linear motion equation of the body based on Newton's differential equation:

$$m_s\ddot{x}_s = f_{l2} + f_{r2} + k_l(x_{ul} - x_s + l_l\theta) + k_r(x_{ur} - x_s - l_r\theta) \quad (1)$$

In this equation, f_{l2} is the force exerted to the left side of the body by the main cylinder of the left side and f_{r2} is the force implemented to the right side of the body from the main right-side cylinder.

The angular motion equation of the body based on the Euler differential equation:

$$I_s\ddot{\theta}_s = -[f_{l2} + k_l(x_{ul} - x_s + l_l\theta)]l_l + [f_{r2} + k_r(x_{ur} - x_s - l_r\theta)]l_r \quad (2)$$

The equation of motion of the left and right side wheels, respectively:

$$m_{ul}\ddot{x}_{ul} = k_{tl}(x_{gl} - x_{ul}) + c_{tl}(\dot{x}_{gl} - \dot{x}_{ul}) - f_{l1} \quad (3)$$

$$m_{ul}\ddot{x}_{ul} = k_{tl}(x_{gl} - x_{ul}) + c_{tl}(\dot{x}_{gl} - \dot{x}_{ul}) - f_{l1} \quad (4)$$

In these relations, f_{l1} is the force exerted on the left wheel by the left main cylinder and f_{r1} is the force exerted on the right wheel by the right main cylinder.

The equation of motion of the left and right side cylinders, respectively:

$$m_c\ddot{x}_{ul} = f_{l1} - k_l(x_{ul} - x_s + l_l\theta) + P_{l2}A_{l2} - P_{l1}A_{l1} \quad (5)$$

$$m_c\ddot{x}_{ur} = f_{r1} - k_r(x_{ur} - x_s - l_r\theta) + P_{r2}A_{r2} - P_{r1}A_{r1} \quad (6)$$

In these equations, P_{l1} and P_{r1} are the lower chamber pressure of the left and right main cylinders, respectively. In addition, P_{l2} and P_{r2} are the upper chamber pressure of the left and right main cylinders, respectively.

The equation of motion of the left and right side pistons, respectively:

$$m_a(\ddot{x}_s - l_l\ddot{\theta}) = -f_{l2} + (P_{l1}A_{l1} - P_{l2}A_{l2}) \quad (7)$$

$$m_a(\ddot{x}_s + l_r\ddot{\theta}) = -f_{r2} + (P_{r1}A_{r1} - P_{r2}A_{r2}) \quad (8)$$

The equation of motion of the left and right side cylinders and pistons together, respectively:

$$m_c\ddot{x}_{ul} + m_a(\ddot{x}_s - l_l\ddot{\theta}) = f_{l1} - f_{l2} - k_l(x_{ul} - x_s + l_l\theta) \quad (9)$$

$$m_c\ddot{x}_{ur} + m_a(\ddot{x}_s + l_r\ddot{\theta}) = f_{r1} - f_{r2} - k_r(x_{ur} - x_s - l_r\theta) \quad (10)$$

By comparing the equations related to the cylinders and pistons motion together and separately, it is observed that the equations derived from motion of both cylinder and piston together are actually the same equations aggregated by those of two separate parts.

2.3 Flow through pipes

Due to the small diameter of the connected tubes between the cylinders and negligible displacement of the wheels due to the small displacement of the cylinder and hydraulic piston, the Reynolds number is much less than 2,000. Therefore, the laminar flow assumption of fluid flow in the tubes between the cylinders is logical. Overall, the fluid flow through the whole hydraulic system (in cylinders and tubes) is presumed laminar. The volumetric flow rate through the tubes is linearly proportional with the pressure difference at two sides of the tube:

$$\Delta Q \propto \Delta P$$

The volumetric flow rate relationship for laminar flow through the tubes between the cylinders can be expressed as:

$$\Delta Q = \frac{\pi D^4}{128\mu L}\Delta P \quad (11)$$

Where, μ is the dynamic viscosity coefficient. Also, combining the relation $Q = A\dot{x}$ with equation (11), the following relation can be articulated:

$$\frac{\pi D^4}{128\mu L}\Delta P = A\dot{x} \quad (12)$$

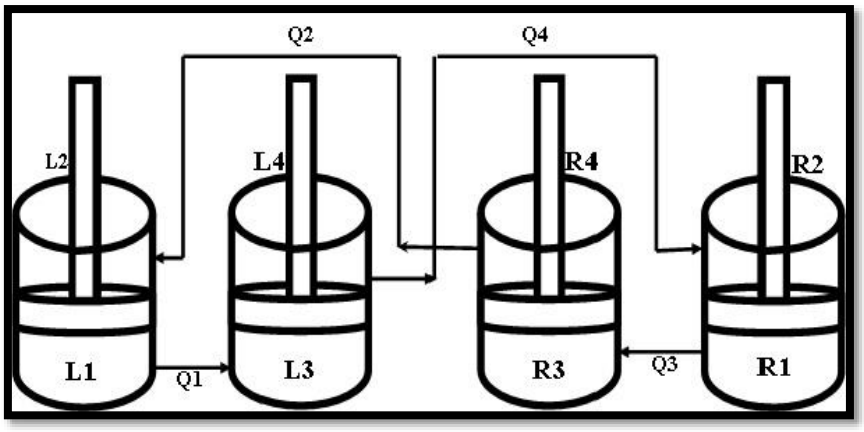

Figure 2 Sketch of four considered hydraulic cylinders for the proposed suspension system.

When numerating, the value of D (diameter of the connected tubes) is considered by default the same in all tubes. In the case of the L (length of the connected tubes), its value in the tubes connecting the adjoining cylinders by default is 1/3 of the value in the tubes connecting the non-adjoining cylinders. The value of μ is unique in all relations since only one fluid is used in all hydraulic systems. According to equation (12), the flow rate relations of the hydraulic tubes between the cylinders are expressed. Overall, there are four hydraulic links, and hence four equations can be written for them. The number of flow rates (Q) and cylinder chambers are based on the numerical value given in figure (2).

Flow through the tubes between the first and third left-hand cylinders (Q_1):

$$\frac{\pi D_1^4}{128\mu l_1}(\mathrm{P_{l1}} - \mathrm{P_{l3}}) = \mathrm{A_{l1}}[\,\dot{x}_{ul} - (\dot{x}_s - l_l\dot{\theta})\,] \tag{13}$$

Flow through the tube between the chamber of the second main left-hand cylinder and the second chamber of the volumetric balanced right-hand cylinder (Q_2):

$$\frac{\pi D_2^4}{128\mu l_2}(\mathrm{P_{r4}} - \mathrm{P_{l2}}) = \mathrm{A_{l2}}[\,\dot{x}_{ur} - (\dot{x}_s + l_r\dot{\theta})\,] \tag{14}$$

Flow through the tube between the first and third chambers of the right-hand cylinders (Q_3):

$$\frac{\pi D_3^4}{128\mu l_3}(\mathrm{P_{r1}} - \mathrm{P_{r3}}) = \mathrm{A_{r1}}[\,\dot{x}_{ur} - (\dot{x}_s + l_r\dot{\theta})\,] \tag{15}$$

Flow through the tube between the chamber of the second main right-hand cylinder and the second chamber of the volumetric balanced left-hand cylinder (Q_4):

$$\frac{\pi D_4^4}{128\mu l_4}(\mathrm{P_{l4}} - \mathrm{P_{r2}}) = \mathrm{A_{r2}}[\,\dot{x}_{ul} - (\dot{x}_s - l_l\dot{\theta})\,] \tag{16}$$

Piston motion equation for the volumetric balanced left- and right-hand hydraulic cylinders, respectively:

$$\mathrm{m_a}(\ddot{\mathrm{x}}_{\mathrm{ul}} - (\ddot{\mathrm{x}}_{\mathrm{s}} - \mathrm{l_l}\ddot{\theta})) = \mathrm{P_{l3}A_{l3}} - \mathrm{P_{l4}A_{l4}} \tag{17}$$

$$\mathrm{m_a}(\ddot{\mathrm{x}}_{\mathrm{ur}} - (\ddot{\mathrm{x}}_{\mathrm{s}} + \mathrm{l_r}\ddot{\theta})) = \mathrm{P_{r3}A_{r3}} - \mathrm{P_{r4}A_{r4}} \tag{18}$$

Flow rate proportionality equation for the main left-hand cylinder:

$$\frac{Q_1}{\mathrm{Q}_2} = \frac{\mathrm{A}_{\mathrm{l}1}}{\mathrm{A}_{\mathrm{l}2}}$$

$$\frac{\frac{\pi D_1^4}{128\mu l_1}(\mathrm{P}_{\mathrm{l}1} - \mathrm{P}_{\mathrm{l}3})}{\frac{\pi D_2^4}{128\mu l_2}(\mathrm{P}_{\mathrm{r}4} - \mathrm{P}_{\mathrm{l}2})} = \frac{\mathrm{A}_{\mathrm{l}1}}{\mathrm{A}_{\mathrm{l}2}}$$

$$\mathrm{A}_{\mathrm{l}2} \times \frac{D_1^4}{l_1}(\mathrm{P}_{\mathrm{l}1} - \mathrm{P}_{\mathrm{l}3}) = \mathrm{A}_{\mathrm{l}1} \times \frac{D_2^4}{l_2}(\mathrm{P}_{\mathrm{r}4} - \mathrm{P}_{\mathrm{l}2}) \tag{19}$$

Flow rate proportionality equation for the main right-hand cylinder:

$$\frac{Q_3}{\mathrm{Q}_4} = \frac{\mathrm{A}_{\mathrm{r}1}}{\mathrm{A}_{\mathrm{r}2}}$$

$$\frac{\frac{\pi D_3^4}{128\mu l_3}(\mathrm{P}_{\mathrm{r}1} - \mathrm{P}_{\mathrm{r}3})}{\frac{\pi D_4^4}{128\mu l_4}(\mathrm{P}_{\mathrm{l}4} - \mathrm{P}_{\mathrm{r}2})} = \frac{\mathrm{A}_{\mathrm{r}1}}{\mathrm{A}_{\mathrm{r}2}}$$

$$\mathrm{A}_{\mathrm{r}2} \times \frac{D_3^4}{l_3}(\mathrm{P}_{\mathrm{r}1} - \mathrm{P}_{\mathrm{r}3}) = \mathrm{A}_{\mathrm{r}1} \times \frac{D_4^4}{l_4}(\mathrm{P}_{\mathrm{l}4} - \mathrm{P}_{\mathrm{r}2}) \tag{20}$$

3 Quaternion neural network controller

Artificial neural networks are able to learn very complex relationships through a massive amount of information and data with similar structure like the human brain [20]. This unique feature has led to widespread use of artificial neural networks in engineering as well as in other sciences. Artificial neural network is used disparately in pivotal applications in engineering science including but not limited to design [21], optimization of various control systems [22], optimal decision making in engineering projects [23], reverse engineering [24], system modeling [25], and identifying errors in industrial and technical systems [26].

In this section, quaternion neural networks have been applied to the inverse kinematic equations of the proposed HIS system. In order to assess the ability of these kinds of controllers, the schematic of different blocks for these controllers is suggested. Schematic of the first block diagram of the control system that uses neural networks is illustrated in figure (3). In this block diagram, the HIS system is located in the forward section. Input to the neural system of the final operator position ($\boldsymbol{p} = \boldsymbol{p_x i} + \boldsymbol{p_y j} + \boldsymbol{p_z k}$) that is achieved by orienting the link ($\boldsymbol{\theta} = \boldsymbol{\theta_0 i} + \boldsymbol{\theta_1 j} + \boldsymbol{\theta_2 k}$) and the predictable output for orientation towards correcting links via quaternion neural networks ($\widetilde{\boldsymbol{\theta}} = \widetilde{\boldsymbol{\theta}}_{\boldsymbol{0}}\boldsymbol{i} + \widetilde{\boldsymbol{\theta}}_{\boldsymbol{1}}\boldsymbol{j} + \widetilde{\boldsymbol{\theta}}_{\boldsymbol{2}}\boldsymbol{k}$) [22]. In the first block diagram, the quaternion neural networks will operate without retrofit capabilities since in this sketch the HIS system is directly connected to the quaternion neural networks and its impact on the system is observable immediately after convergence of the solutions.

To improve the first block diagram performance, the second schematic is considered and depicted in figure (4). Input of the control system is the desirable position in the HIS system ($\boldsymbol{p} = \boldsymbol{p_{dx} i} + \boldsymbol{p_{dy} j} + \boldsymbol{p_{dz} k}$) and the output is prediction of the neural networks from the modified link direction ($\widetilde{\boldsymbol{\theta}}$). $\widetilde{\boldsymbol{\theta}}$ is actually derived from a comparison of the final position ($\boldsymbol{p}$) and the modified position ($\boldsymbol{p_d}$).

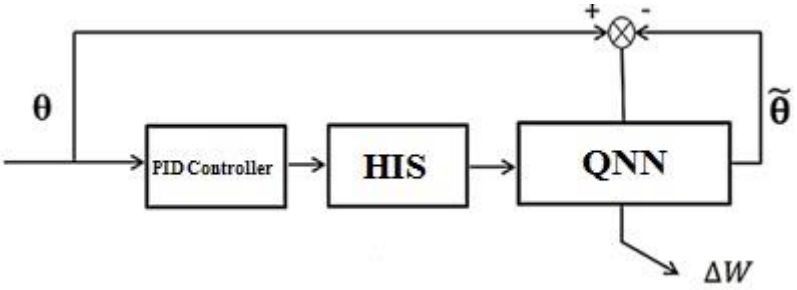

Figure 3 Schematic of the first block diagram of the quaternion neural network controller.

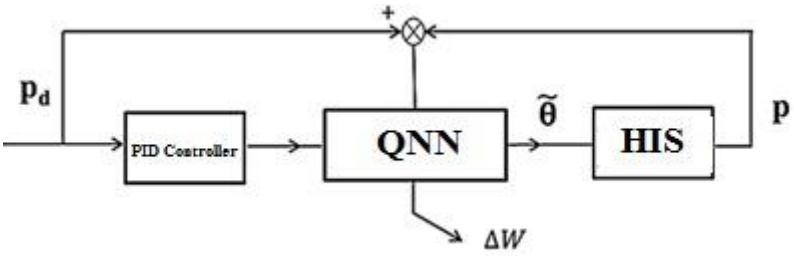

Figure 4 Schematic of the second block diagram of the quaternion neural network controller.

In the new sketch, $\boldsymbol{p_d}$ also provides a regular maintenance of position in the Cartesian space. In accordance with the quaternion reversible algorithm, the update relation can be expressed as follows [27]:

$$\Delta \boldsymbol{W} = \sum_{\boldsymbol{n=x,y,z}} \boldsymbol{\mu}\left(-\frac{\boldsymbol{\partial J}}{\boldsymbol{\partial p_n}}\frac{\boldsymbol{\partial p_n}}{\boldsymbol{\partial Y_k}}\frac{\boldsymbol{\partial Y_k}}{\boldsymbol{\partial W}}\right) \tag{21}$$

Where, $\boldsymbol{Y_k}$ is the kth output of the quaternion neural network and $\frac{\boldsymbol{\partial p_n}}{\boldsymbol{\partial Y_k}}$ is the Jacobian system. When the functions of the HIS system are known, the Jacobian of the system can be calculated by deriving the functions associated with each input.

However, some other methods are used to estimate dynamical functions when the functions of the HIS system has not been determined [28]. One of these methods is the artificial quaternion neural network to estimate equations, which is also referred to as the topology of special learning in neural network [27].

In this scheme, two quaternion neural networks have been used. The first quaternion neural network is a controller to estimate the kinematics of the HIS system, whilst the second quaternion neural network is used to predict the functions of the system. This sketch can outstrip without modifying the controller as it is connected to different systems.

4 Simulation of the proposed suspension system using MATLAB®(V.8.1)/Simulink software

It is imperious to present a cohesive mathematical model of the investigated systems in the Simulink for simulation purposes. In Simulink, physical models are depicted in terms of graphics and block diagrams [5]. Simulink is numerically able to estimate responses of mathematical models that cannot be solved manually or analytically [12]. In this section, the Simulink and Simscape (sub-sections of SimMechanics and SimHydraulics) libraries in MATLAB® (V.8.1)/Simulink software have been used [4].

First and foremost, the half car model in the transverse direction with a passive suspension system (conventional suspension system with constant spring and damping coefficients) will be simulated and analyzed. In the following, the half car model in the transverse direction with a HIS system and a QNN controller is simulated and analyzed and its merits versus of the passive suspension system is extensively discussed.
Also, the response of wheels and body with respect to road bumps in both of the above-mentioned suspension systems are outlined and discussed.

4.1 Validation

In this section, the experimental results of Zhang et al. [9] have been used to show the accuracy of present simulation. Figure (5) depicts variations of the frequency response of the right wheel, bounce, and rolling in the vertical direction. As can be seen, the difference in results is less than 10% in all frequencies, which indicates the acceptable accuracy of the simulation.

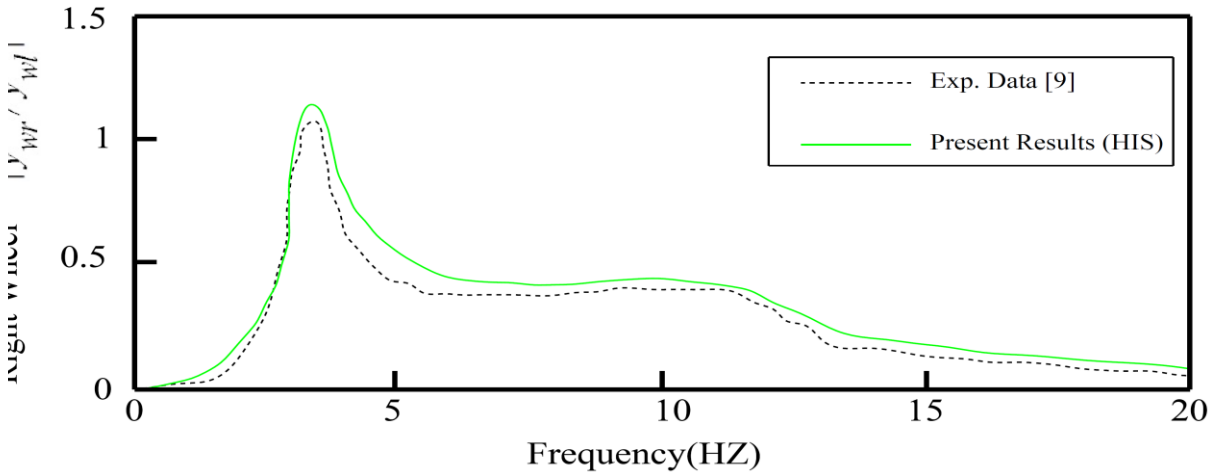

(**a**)

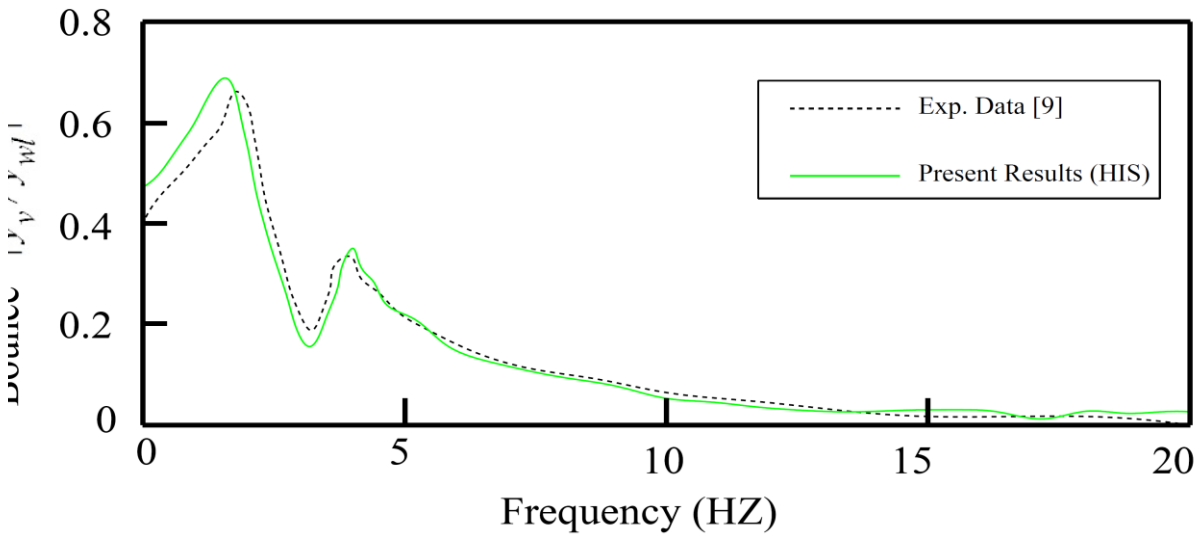

(**b**)

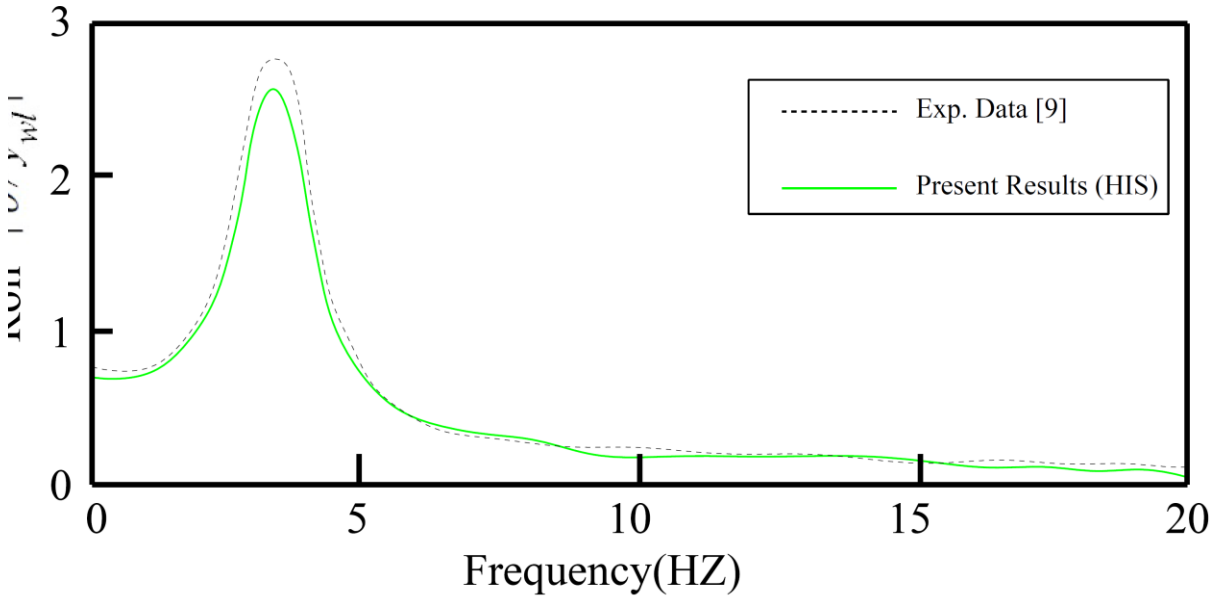

(**c**)

Figure 5 Model verification between present study and experimental results of Zhang et al. [9] for: (a) the frequency response of the right wheel, (b) bounce, and (c) rolling in the vertical direction.

4.2 Half car model in transverse direction with the passive suspension system

In this section, spring and shock absorber systems are used to model the wheel tires and the passive suspension system as well (Figure (6)) [29]. Also, a homogeneous and wide rod-shaped body that only has an inertia moment in the perpendicular direction of the plane (along the Z-axis) is used to model the body [18]. In the SimMechanics, simulation is usually accompanied with initial oscillations, until the model reaches a stable condition [30]. Therefore, the input is employed after damping of the initial oscillation (here, from the third second onward).

To simulate the model, the height of the obstacle and the speed of the car (as passing from the obstacle) are assumed 10 cm and 54 km/h, respectively.

According to the height of the obstacle, the assumed speed is an excellent performance indicator of the suspension system at a relatively critical condition. In both models investigated in this paper, the x-axis is presumed along the vehicle's width, the y-axis is in the vehicle's height direction, and the z-axis is outwardly perpendicular to the plate [31]. The center of the coordinates is also located on the left and bottom of the sketch (exactly below the left-hand wheel).

According to figure (5), the input signal is fed to the wheel set-up via a joint actuator. In this method, all three curves of the position-time, speed-time, and acceleration-time (as inputs) are initially supplied to the system (Figure (7)). All three curves are combined through a Mux block and then entered to the joint actuator via a line.

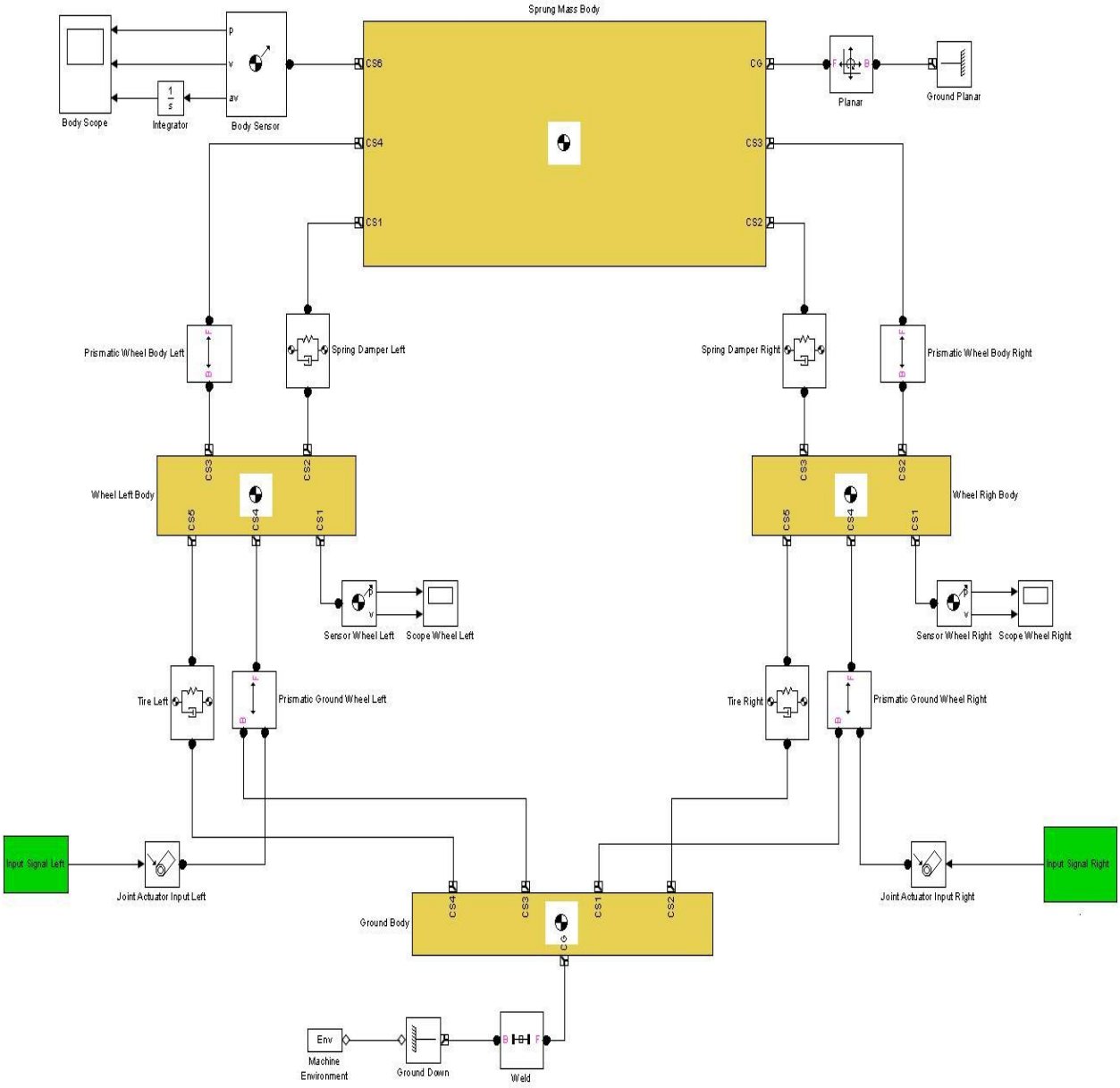

Figure 6 Half car model in the transverse direction with the passive suspension system.

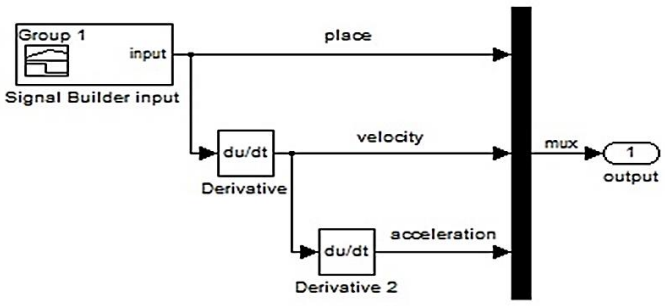

Figure 7 Input elements between the left wheel and earth.

Table 1 Input data for the suspension system of the vehicle [11].

Parameter	Unit	Value
Mass of vehicle, m_s	kg	690
Right-hand unsprung mass, m_{ur}	kg	35
Spring stiffness of the right-hand suspension system, K_{sr}	N/m	18,000
Hardness coefficient of right-hand wheel, K_{tr}	N/m	200,000
Damping coefficient of the right-hand suspension shock absorber, C_{sr}	N.s/m	1,500
Damping coefficient of the right-hand wheel, C_{tr}	N.s/m	400
Transversal distance of gravity center of the body and right-hand suspension system, l_r	m	1
Height of obstacle from right-hand wheel, X_{gr}	m	0.1
Track distance, T	m	2
Gravity acceleration, g	m/s^2	9.81
Car speed when passing the obstacle, V	m/s	15
Distance of chassis from road surface, y_1	m	0.64
Radius of car wheel, r	m	0.2
Unsprung mass (left-hand), m_{ul}	kg	35
Spring stiffness coefficient of the left-hand suspension system, K_{sl}	N/m	18,000
Hardness coefficient of left-hand wheel, K_{tl}	N/m	200,000
Damping coefficient of the left-hand suspension shock absorber, C_{sl}	N.s/m	1,500
Damping coefficient of the left-hand wheel, C_{tl}	N.s/m	400
Transversal distance between the gravity center of the body and left-hand suspension system, l_l	m	1
Height of obstacle from left-hand wheel, X_{gl}	m	0.1

4.3 Half car model in transverse direction with the HIS system

In this model, the configuration of the springs, masses, the characteristics of the tires and the left and right inputs are similar to the passive suspension system. In this layout, four double-sided hydraulic cylinders with interconnected pipes and connections between them instead of the conventional shock absorbers are used [32]. The body of the main hydraulic cylinders is connected to the wheel hub from the bottom, whilst the piston is connected directly to the body from the upper part. In this design, the body of the volume balanced hydraulic cylinder is welded to an appropriate point of the chassis or body, while the piston of these cylinders are not connected anywhere and move freely (Figure (8)).

In this model, the connection between the body and the wheels is considered linear, and hence springs with a linear joint attachment are used. The body, like the passive suspension system, has two degrees of freedom (vertical and angular motion).
The blocks of the wheels vibrate vertically and are directly influenced by motion of the body of the left and right hydraulic cylinders.

This model has two solvers, namely the Simulink and SimMechanics solver (which is Ode15s), and the other is the SimHydraulics, which is actually a local solver. In the SimHydraulics solver, the inverse Euler based on the quaternion neural network method is available which is used in this study (Figure (9)).

In this system, the hardness of the spring connected to the balanced hydraulic cylinder is assumed approximately zero (0.000001 N/m) and the initial deformation is set to zero. In order to consider the coulomb and viscous friction caused by the slip of fluid layers over the surface of each other and solid, the friction block is connected to the hydraulic cylinders in parallel. In this suspension system, rigid pipes with circular cross-section are used [6]. The inner diameter of the pipe is 7 mm and the initial pressure is 1 atmosphere [8].

As shown in figure (2), the length of the hydraulic tube of the adjoining chambers (Q1, Q3) is assumed 0.5 m and the length of the hydraulic tube of the apart chambers (Q2, Q4) is presumed 1.5 m. The hydraulic fluid used in this system is also a brake fluid with five US departments of Transportation (DOTs) [33]. This oil is extremely hydrophobia and has a low viscosity.

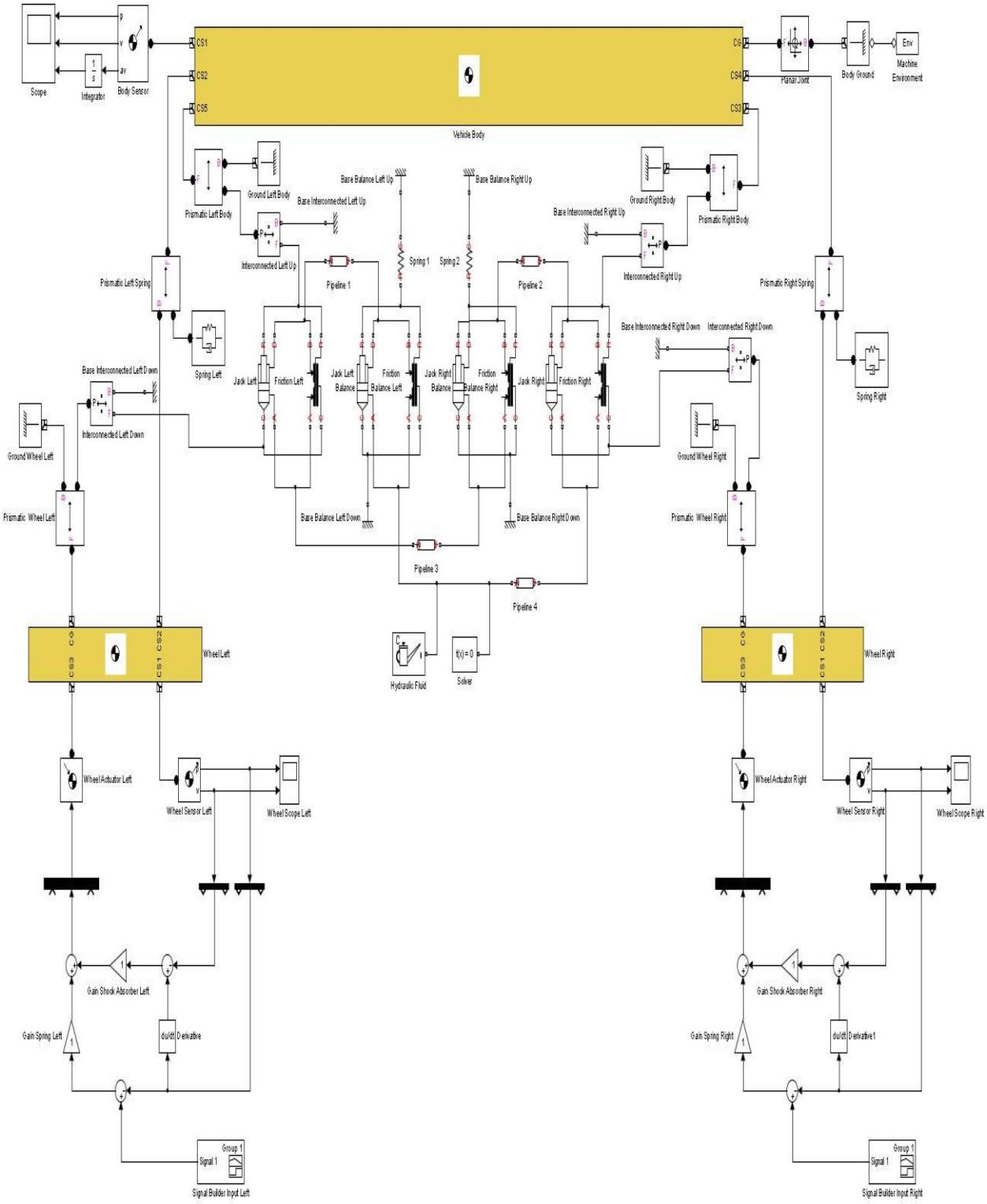

Figure 8 Half car model in the transverse direction with the HIS system.

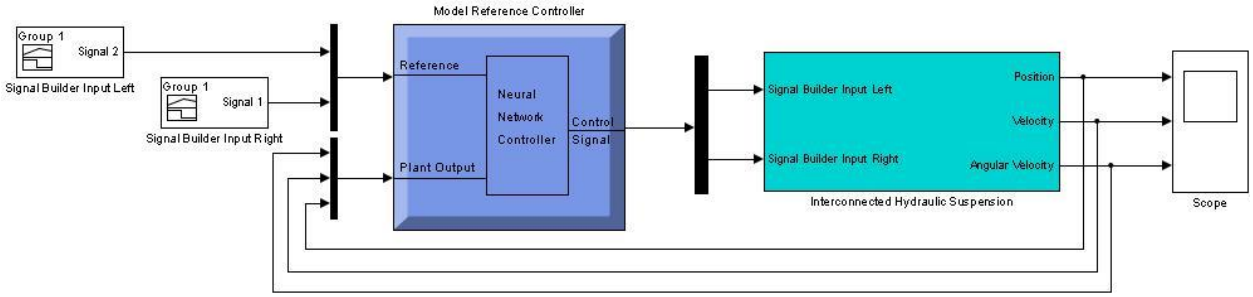

Figure 9 The HIS system and quaternion neural network controller.

5 Results and discussion of simulation

Comparison Analysis In order to illustrate the dynamic performance of the vehicle with HIS-QNN, simulations are taken into account. In this manner, the stochastic road is selected as the excitation of the vehicle with HIS-QNN and the vehicle parameters are initialized as in Table (1). Moreover, the HIS-QNN dynamics are compared to those of the conventional suspension system. The dynamics of both suspension systems are shown in figure (10). The results suggested that HIS-QNN can resist the Roll motion and it can also maintain good ride performance what makes the HIS-QNN is slightly better than the conventional suspension.

The dynamic response of the body and the right and left wheels to the hardness of the road surface are considered as effective factors in evaluation of the suspension system. In analysis, the right wheel will always pass through the obstacle. Due to the fact that the initial oscillations, caused by weight of the body and wheels, are less important for understanding the properties of the vehicle, all sketches have been displayed from the third second onward. In all figures, there are three curves each with different colors. Black color indicates the curve of the passive suspension system, green color indicates the curve of the HIS suspension system, and blue color indicates the curve of the HIS suspension system with a quaternion neural network controller. In the hydraulic suspension system the oscillation amplitude in all diagrams is reduced compared to the passive suspension system due to the interconnection between the chamber of the hydraulic cylinders and the coupling of the wheels with each others.

Also, in all diagrams, the response of the HIS system with a quaternion neural network controller is smoother than other systems, which improves the stability of the vehicle.

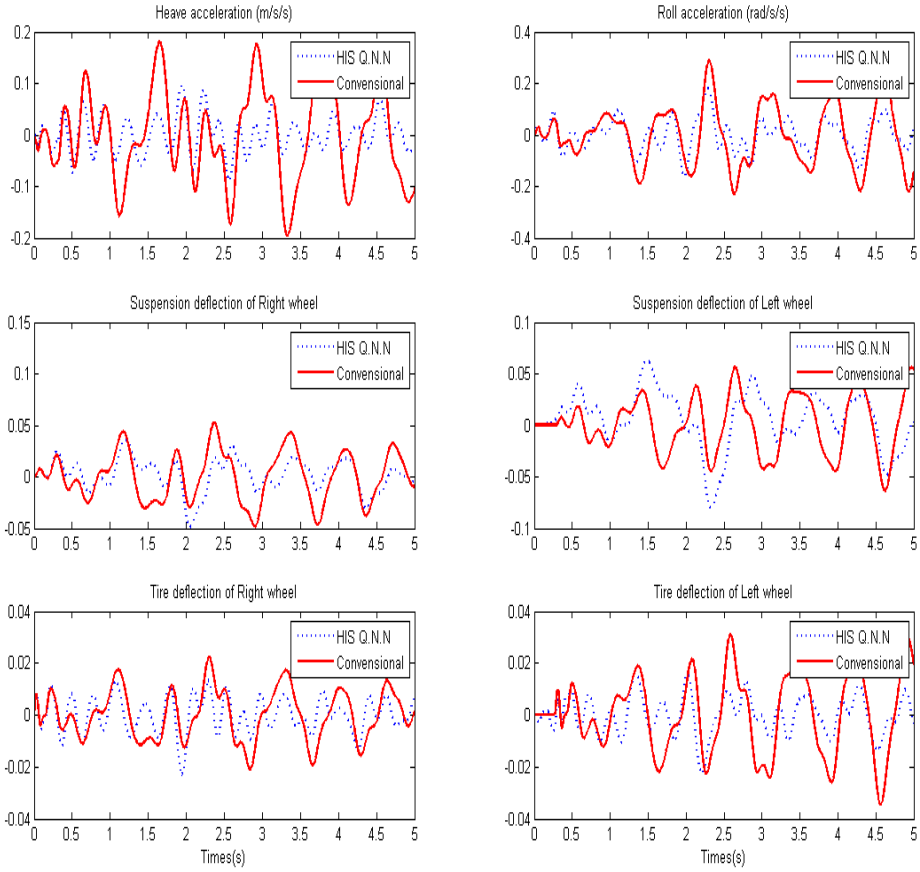

Figure 10 The comparison between the conventional suspension system and the HIS-QNN.

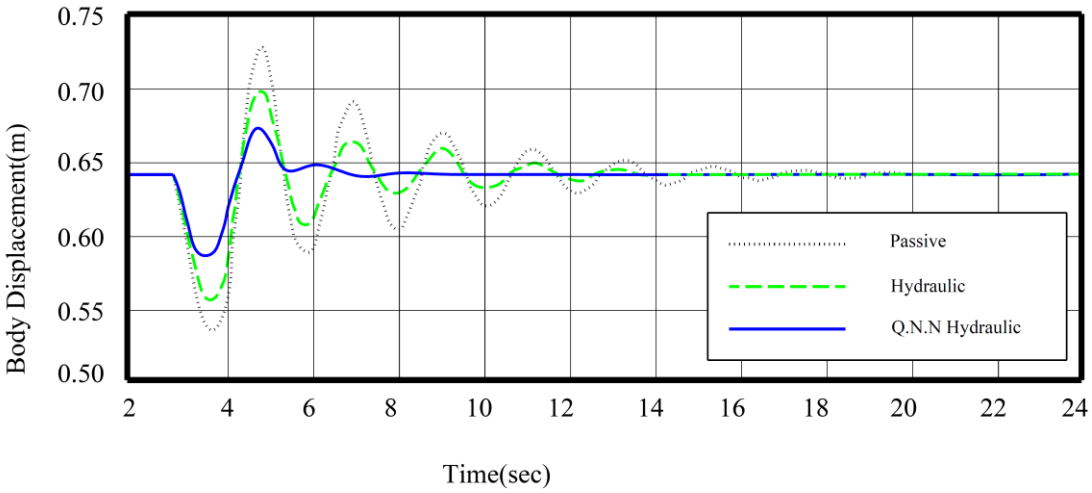

Figure 11 The body response for three examined suspension systems when both wheels pass the obstacle.

As figure (11) exhibits, the maximum peak overshoot of the body when both wheels pass through the obstacle is 0.73 m for the passive suspension system, 0.7 m for the HIS system and 0.67 m for the HIS system with a quaternion neural network controller.

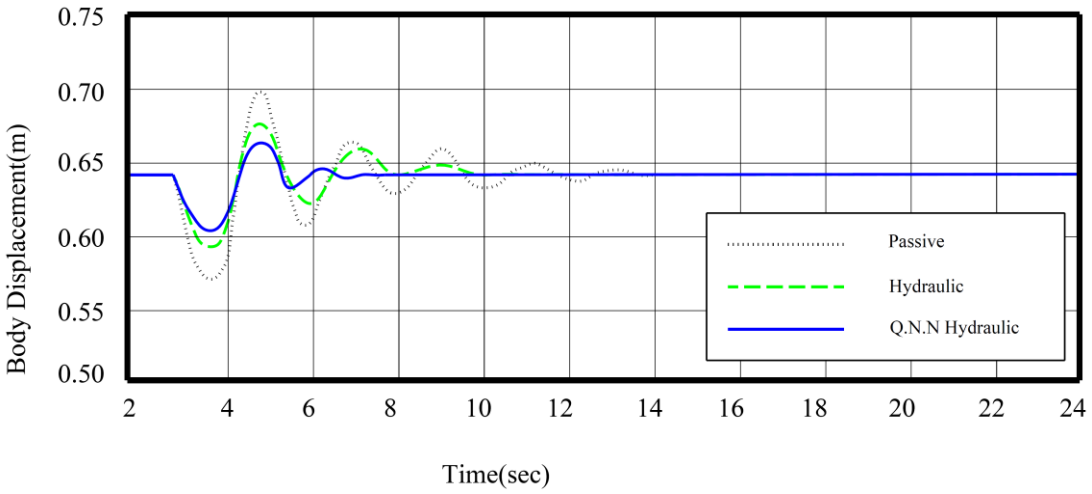

Figure 12 The body response for three examined suspension systems when only right wheel passes the obstacle.

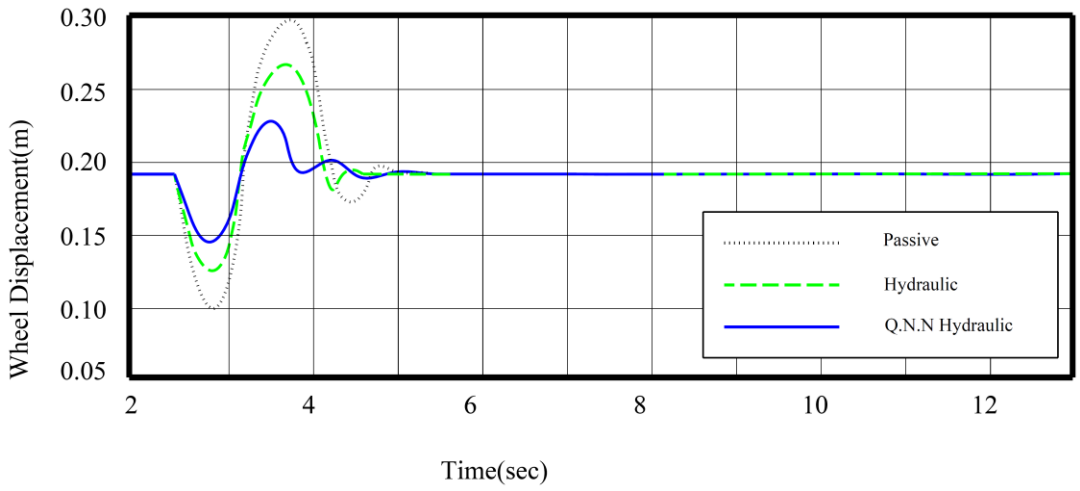

Figure 13 The left or right wheel response for three examined suspension systems when two wheels pass the obstacle.

As figure (12) exhibits, the maximum peak overshoot of the body when only right wheel passes through the obstacle is 0.7 m for the passive suspension system, 0.67 m for the HIS system and 0.66 m for the HIS system with a quaternion neural network controller.

As figure (13) indicates, the maximum peak overshoot of the left or right wheel when both wheels pass through the obstacle is 0.3 m for the passive suspension system, 0.27 m for the HIS system and 0.23 m for the HIS system with a quaternion neural network controller.

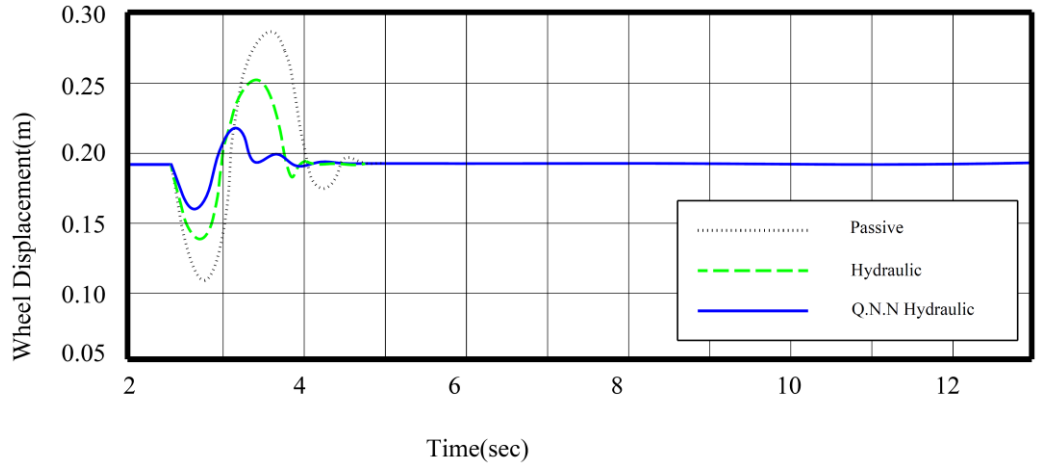

Figure 14 The right wheel response for three examined suspension systems when only right wheel passes the obstacle.

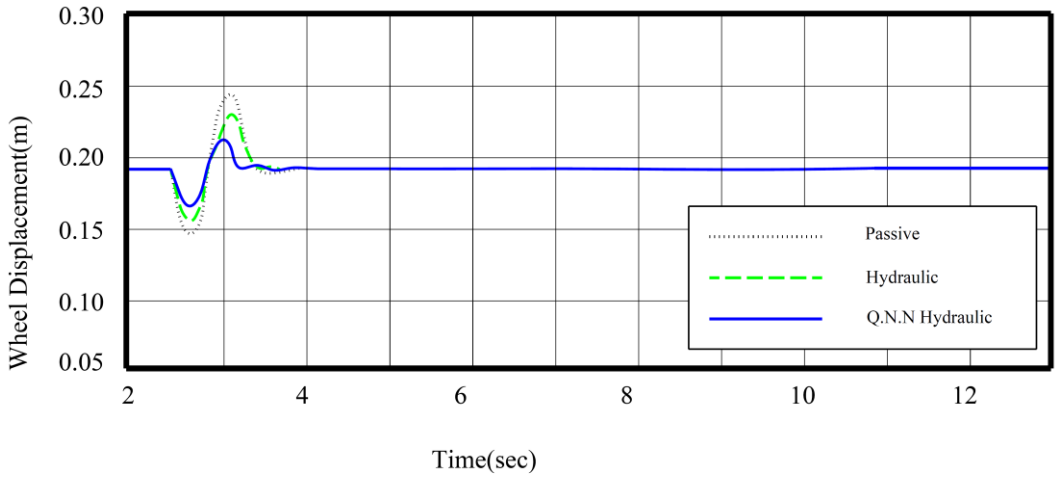

Figure 15 The left wheel response for three examined suspension systems when only right wheel passes the obstacle.

As figure (14) displays, the maximum peak overshoot of the right wheel when only right wheel passes through the obstacle is 0.29 m for the passive suspension system, 0.25 m for the HIS system and 0.22 m for the HIS system with a quaternion neural network controller.
As figure (15) portrays, the maximum peak overshoot of the left wheel when only right wheel passes through the obstacle is 0.24 m for the passive suspension system, 0.23 m for the HIS system and 0.21 m for the HIS system with a quaternion neural network controller.

6 Concluding remarks

Continued previous research [34-36], in this paper, the paramount significance of the hydraulic interconnected suspension system with a quaternion neural network controller in the stability of a vehicle is thoroughly discussed. The results of simulation carried out by MATLAB® (V.8.1)/Simulink software demonstrated that the implementation of the quaternion neural network controller on the hydraulic interconnected suspension system reduces the displacement amplitude of the body and wheel in the exposure to the bumps of the road.

The maximum peak overshoot of the body when both wheels pass through the obstacle (Figure (11)) for the HIS system with a quaternion neural network controller is 8% less than the passive suspension system. The ride comfort of the passengers is also improved with the use of this controller. The comparison of the diagrams exhibited that the HIS system has a high ability to redress the balance when a wheel passes through an obstacle.
Also, the damping of oscillation in this system is high. This indicates that, after the first oscillation, the next oscillations amplitude will be dramatically reduced. Regarding the discussed scenarios and the consequences that the HIS system is provided for the considered vehicle, selecting the quaternion neural network controller improves the stability of the vehicle.

References

[1] Baumal, A. E., Mcphee, J. J., and Calamai, P. H., "Application of Genetic Algorithms to the Design Optimization of an Active Vehicle Suspension System", Computer Methods in Applied Mechanics and Engineering Journal, Vol. 163, pp. 87-94, (1998).

[2] Chen, B. C., Shiu, Y. H., and Hsieh, F. C., "Sliding-mode Control for Semi-active Suspension with Actuator Dynamics", Vehicle System Dynamics, Vol. 49, pp. 277-290, (2011).

[3] Abdelkareem, M. A., Xu, L., Ali, M. K. A., Elagouz, A., Mi, J., and Guo, S., "Vibration Energy Harvesting in Automotive Suspension System: A Detailed Review", Applied Energy, Vol. 229, pp. 672-699, (2018).

[4] Omar, M., El-Kassaby, M., and Abdelghaffar, W., "A Universal Suspension Test Rig for Electrohydraulic Active and Passive Automotive Suspension System", Alexandria Engineering Journal, Vol. 56, pp. 359-370, (2017).

[5] Phalke, T. P., and Mitra, A. C., "Analysis of Ride Comfort and Road Holding of Quarter Car Model by Simulink", Materials Today: Proceedings, Vol. 4, pp. 2425-2430, (2017).

[6] Miller, L. R., and Nobles, C. M., "The Design and Development of a Semi-active Suspension for a Military Tank", SAE Technical Paper 0148-7191, (1988).

[7] Yao, Z., " Design and Analysis of an Interconnected Suspension for a Small Off-road Vehicle", M.Sc. Thesis, University of Windsor, Canada, (2016).

[8] Esfahani, M. I. M., Mosayebi, M., Pourshams, M., and Keshavarzi, A., "Optimization of Double Wishbone Suspension System with Variable Camber Angle by Hydraulic Mechanism", World Academy of Science, Engineering and Technology, Vol. 61, pp. 299-306, (2010).

[9] Smith, W., Zhang, N., and Jeyakumaran, J., "Hydraulically Interconnected Vehicle Suspensions: Theoretical and Experimental Ride Analysis", Veh. Syst Dyn., Vol. 48, pp. 41-64, (2010).

[10] Cao, D., Rakheja, S., and Su, C. Y., "A Generalized Model of a Class of Interconnected Hydro-pneumatic Suspensions and Analysis of Pitch Properties", in ASME 2006 International Mechanical Engineering Congress and Exposition, pp. 137-146, (2006).

[11] Zhu, H., Yang, J., and Zhang, Y., "Modeling and Optimization for Pneumatically Pitch-Interconnected Suspensions of a Vehicle", Journal of Sound and Vibration, Vol. 432, pp. 290-309, (2018).

[12] Zou, J., Guo, X., Xu, L., Abdelkareem, M. A., Gong, B., and Zhang, J., "Simulation Research of a Hydraulic Interconnected Suspension Based on a Hydraulic Energy Regenerative Shock Absorber", SAE Technical Paper 0148-7191, (2018).

[13] Shengzhao, C., Yixu, Z., Bangji, Z., and Nong, Z., "Influence of Key Parameters of Hydraulically Interconnected Suspension on Vehicle Dynamics and Experimental Validation", Journal of Mechanical Engineering, Vol. 53, pp. 1-224 2017-07-20, (2017).

[14] Bouazara, M., and Richard, M. J., "An Optimization Method Designed to Improve 3-D Vehicle Comfort and Road Holding Capability Through the use of Active and Semi-active Suspensions", European Journal of Mechanics-A/Solids, Vol. 20, pp. 509-520, (2001).

[15] Bagheri, A., Mahmoodabadi, M., Rostami, H., and Kheybari, Sh., "Pareto Optimization of a Two-degree of Freedom Passive Linear Suspension using a New Multi-objective Genetic Algorithm", International Journal of Engineering, (2011).

[16] Nariman-Zadeh, N., Salehpour, M., Jamali, A., and Haghgoo, E., "Pareto Optimization of a Five-degree of Freedom Vehicle Vibration Model using a Multi-objective Uniform-Diversity Genetic Algorithm (MUGA)", Engineering Applications of Artificial Intelligence, Vol. 23, pp. 543-551, (2010).

[17] Thompson, A., "The Effect of Tyre Damping on the Performance of Vibration Absorbers in an Active Suspension", Journal of Sound and Vibration, Vol. 133, pp. 457-465, (1989).

[18] Omar, M., El-kassaby, M. M., and Abdelghaffar, W., "Parametric Numerical Study of Electrohydraulic Active Suspension Performance Against Passive Suspension", Alexandria Engineering Journal, Vol. 57, No. 4, pp. 3609–3614, Dec. (2018).

[19] Ma, X., Wong, P. K., and Zhao, J., "Practical Multi-objective Control for Automotive Semi-active Suspension System with Nonlinear Hydraulic Adjustable Damper", Mechanical Systems and Signal Processing, Vol. 117, pp. 667-688, (2019).

[20] Tu, Z., Zhao, Y., Ding, N., Feng, Y., and Zhang, W., "Stability Analysis of Quaternion-Valued Neural Networks with both Discrete and Distributed Delays", Applied Mathematics and Computation, Vol. 343, pp. 342-353, (2019).

[21] Spentzas, K., and Kanarachos, S. A., "Design of a Non-linear Hybrid Car Suspension System using Neural Networks", Mathematics and Computers in Simulation, Vol. 60, pp. 369-378, (2002).

[22] Pang, H., Liu, F., and Xu, Z., "Variable Universe Fuzzy Control for Vehicle Semi-active Suspension System with MR Damper Combining Fuzzy Neural Network and Particle Swarm Optimization", Neurocomputing, Vol. 306, pp. 130-140, (2018).

[23] Monedero, I., Biscarri, F., León, C., Guerrero, J. I., González, R., and Pérez-Lombard, L., "Decision System Based on Neural Networks to Optimize the Energy Efficiency of a Petrochemical Plant," Expert Systems with Applications, Vol. 39, pp. 9860-9867, (2012).

[24] Floares, A. G., "A Reverse Engineering Algorithm for Neural Networks, Applied to the Subthalamopallidal Network of Basal Ganglia", Neural Networks,Vol. 21, pp. 379-386, (2008).

[25] Huang, F., Zhao, C., Huang, Y., Dai, P., Hao, D., and Yue, Y., "Study on the Evaluation Model of Vehicle Comfort Based on the Neural Network", IFAC-PapersOnLine, Vol. 51, pp. 553-558, (2018).

[26] Luo, H., Huang, M., and Zhou, Z., "Integration of Multi-Gaussian Fitting and LSTM Neural Networks for Health Monitoring of an Automotive Suspension Component", Journal of Sound and Vibration, Vol. 428, pp. 87-103, (2018).

[27] Takahashi, K., Hasegawa, Y., and Hashimoto, M., "Design of Quaternion-Neural-Network-Based Self-Tuning Control Systems", Sensors and Materials, Vol. 29, pp. 699-711, (2017).

[28] Eslaminasab, N., "Development of a Semi-active Intelligent Suspension System for Heavy Vehicles", Ph.D. Thesis, University of Waterloo, Canada, (2008).

[29] Wei, C., and Taghavifar, H., "A Novel Approach to Energy Harvesting from Vehicle Suspension System: Half-vehicle Model", Energy, Vol. 134, pp. 279-288, (2017).

[30] Tandel, A., Deshpande, A., Deshmukh, S., and Jagtap, K., "Modeling, Analysis and PID Controller Implementation on Double Wshbone Suspension using Simmechanics and Simulink", Procedia Engineering, Vol. 97, pp. 1274-1281, (2014).

[31] Boada, B. L., Boada, M. J. L., Vargas-Melendez, L., and Diaz, V., "A Robust Observer Based on H∞ Filtering with Parameter Uncertainties Combined with Neural Networks for Estimation of Vehicle Roll Angle", Mechanical Systems and Signal Processing, Vol. 99, pp. 611-623, (2018).

[32] Guo, S., Chen, Z., Guo, X., Zhou, Q., and Zhang, J., "Vehicle Interconnected Suspension System based on Hydraulic Electromagnetic Energy Harvest: Design, Modeling and Simulation Tests", SAE Technical Paper 0148-7191, (2014).

[33] Jazar, R. N., "*Vehicle Dynamics: Theory and Application*", Springer, (2017).

[34] Bakkhoshnevis, A. A., Mamouri, A. R., and Nazari, S., "Experimental Investigation of Wake on an Elliptic Cylinder in the Presence of Tripping Wire", Iranian Journal of Mechanical Engineering, Transactions of the ISME, Vol. 18, pp. 81-102, (2017).

[35] Bakkhoshnevis, A. A., Mamouri, A. R., and Khodadadi, M., " Experimental Investigation for Wake of the Circular Cylinder by Attaching Different Number of Tripping Wires", Iranian Journal of Mechanical Engineering, Transactions of the ISME, Vol. 17, pp. 5-25, (2016).

[36] Mamouri, A. R., Khoshnevis, A. B., and Lakzian, E., " Entropy Generation Analysis of S825, S822, SD7062 Offshore Wind Turbine Airfoil Geometries", Ocean Engineering, Vol. 173, pp. 700-715, (2019).

[37] Mamouri, A. R., Lakzian, E., and Khoshnevis, A. B., " Entropy Analysis of Pitching Airfoil for Offshore Wind Turbines in the Dynamic Stall Condition", Ocean Engineering, Vol. 187, pp. 106229, (2019).

Nomenclature

m_s: Mass of vehicle (kg)
m_{ul}: Left-hand unsprung mass (kg)
m_{ur}: Right-hand unsprung mass (kg)
m_c: Mass of cylinder (kg)
m_a: Mass of piston (kg)
T: Track distance (m)
g: Gravity acceleration ($m.s^{-2}$)
V: Car speed when passing the obstacle ($m.s^{-1}$)
y_1: Distance of chassis from road surface (m)
r: Radius of car wheel (m)
θ: Roll Angle (Rad)
$\ddot{\theta}_s$: Angular Acceleration ($Rad.s^{-2}$)
I_s: Moment of inertia ($kg.m^2$)
x_s: vertical linear motion of the body (m)
$\ddot{x}_s$: vertical linear acceleration of the body ($m.s^{-2}$)
x_{ul}: vertical linear motion of left-hand wheel (m)
x_{ur}: vertical linear motion of right-hand wheel (m)
$\dot{x}_{ul}$: vertical linear velocity of left-hand wheel ($m.s^{-1}$)
$\dot{x}_{ur}$: vertical linear velocity of right-hand wheel ($m.s^{-1}$)
$\ddot{x}_{ul}$: vertical linear acceleration of left-hand wheel ($m.s^{-2}$)
$\ddot{x}_{ur}$: vertical linear acceleration of right-hand wheel ($m.s^{-2}$)
f_{l1}: the force exerted on the left wheel by the left main cylinder (N)
f_{r1}: the force exerted on the right wheel by the right main cylinder (N)
f_{l2}: the force exerted to the left side of the body by the main cylinder of the left side (N)
f_{r2}: the force exerted to the right side of the body from the main right-side cylinder (N)
l_l: Transversal distance of gravity center of the body and left-hand suspension system (m)
l_r: Transversal distance of gravity center of the body and right-hand suspension system (m)
k_{tl}: Hardness coefficient of left-hand wheel ($N.m^{-1}$)
k_{tr}: Hardness coefficient of right-hand wheel ($N.m^{-1}$)
K_{sl}: Spring stiffness of the left-hand suspension system ($N.m^{-1}$)
K_{sr}: Spring stiffness of the right-hand suspension system ($N.m^{-1}$)
C_{sl}: Damping coefficient of the left-hand suspension shock absorber ($N.s.m^{-1}$)
C_{sr}: Damping coefficient of the right-hand suspension shock absorber ($N.s.m^{-1}$)
C_{tl}: Damping coefficient of the left-hand wheel ($N.s.m^{-1}$)
C_{tr}: Damping coefficient of the right-hand wheel ($N.s.m^{-1}$)
x_{gl}: Height of obstacle from left-hand wheel (m)

x_{gr}: Height of obstacle from right-hand wheel (m)
P_{l1}: lower compartment pressure inside the main cylinder on the left ($N.m^{-2}$)
P_{l2}: upper compartment pressure inside the main cylinder on the left ($N.m^{-2}$)
P_{l3}: lower compartment pressure inside the volumetric balanced cylinder on the left ($N.m^{-2}$)
P_{l4}: upper compartment pressure inside the volumetric balanced cylinder on the left ($N.m^{-2}$)
P_{r1}: lower compartment pressure inside the main cylinder on the right ($N.m^{-2}$)
P_{r2}: upper compartment pressure inside the main cylinder on the right ($N.m^{-2}$)
P_{r3}: lower compartment pressure inside the volumetric balanced cylinder on the right ($N.m^{-2}$)
P_{r4}: upper compartment pressure inside the volumetric balanced cylinder on the right ($N.m^{-2}$)
A_{l1}: lower compartment cross section inside the main cylinder on the left (m^2)
A_{l2}: upper compartment cross section inside the main cylinder on the left (m^2)
A_{l3}: lower compartment cross section inside the volumetric balanced cylinder on the left (m^2)
A_{l4}: upper compartment cross section inside the volumetric balanced cylinder on the left (m^2)
A_{r1}: lower compartment cross section inside the main cylinder on the right (m^2)
A_{r2}: upper compartment cross section inside the main cylinder on the right (m^2)
A_{r3}: lower compartment cross section inside the volumetric balanced cylinder on the right (m^2)
A_{r4}: upper compartment cross section inside the volumetric balanced cylinder on the right (m^2)
ΔQ: volumetric flow rate ($m^3.s^{-1}$)
ΔP: pressure difference ($N.m^{-2}$)
D: diameter of the connected tubes (m)
μ: dynamic viscosity coefficient ($N.m^{-2}.s$)
L: length of the connected tubes (m)
π: pi (3.14159)
ΔW: quaternion reversible algorithm
Y: output of the quaternion neural network